Neutron-scattering study of the two-dimensional frustrated antiferromagnet $Rb_2Cu_{0.12}Co_{0.88}F_4$

A. G. Schins
Faculty of Physics and Astronomy and Debye Institute, Utrecht University, P.O. Box 80000, 3508 TA Utrecht, The Netherlands

M. Nielsen
Physics Department, Risø National Laboratory, P.O. Box 49, DK-4000 Roskilde, Denmark

A. F. M. Arts and H. W. de Wijn
Faculty of Physics and Astronomy and Debye Institute, Utrecht University, P.O. Box 80000, 3508 TA Utrecht, The Netherlands

(Received 14 June 1993)

Quasielastic neutron scattering is performed on a single crystal of the two-dimensional antiferromagnet $Rb_2Cu_{0.12}Co_{0.88}F_4$, whose magnetic structure is frustrated by the admixture of ferromagnetic bonds. From the critical scattering, the in-plane inverse correlation length is found to decrease linearly with the temperature, with a critical exponent $\nu = 1.02 \pm 0.04$. At the onset of the sublattice magnetization, which occurs at $T_N = 88.1 \pm 0.1$ K, however, the in-plane correlations have not yet become long ranged. At T_N, the planar domain size has grown to only 14 lattice spacings. Below T_N, the planar domains size increases further, to attain length scales beyond resolution at about 75 K. Conversely, the domains break up into smaller ones in this temperature range upon warming up. For the critical exponent of the susceptibility we find $\gamma = 1.5 \pm 0.2$ after correction for the finite correlation remaining at T_N. The sublattice magnetization obeys the critical exponent $\beta = 0.16 \pm 0.04$. The critical exponents found compare with the Ising values $\nu = 1$, $\gamma = \frac{7}{4}$, and $\beta = \frac{1}{8}$. Another manifestation of the frustration is the failure to reach true equilibrium below T_N. This is reflected in a dependence of the c-axis correlations on the cooling rate, and in a small increment of the intralayer and in-layer correlation lengths over long times.

I. INTRODUCTION

$Rb_2Cu_{1-x}Co_xF_4$ belongs to the family of two-dimensional (2D) magnetic systems with the so-called K_2NiF_4 structure. The magnetic ions are arranged in quadratic layers, and the primary interaction within the layers is exchange between nearest neighbors. The interactions among adjacent layers are many orders of magnitude smaller than those within the layers, and in the antiferromagnets these interactions furthermore nearly perfectly cancel because of the symmetry. In fact, the quadratic-layer magnets have been established to be archetypes of genuinely 2D behavior, with the magnetic transition occurring at a finite temperature because of anisotropy.[1] In the vicinity of the transition furthermore a crossover to 3D has been observed, which is ascribed to the fact that the small but finite interlayer interactions (in antiferromagnets predominantly between next-nearest layers) integrate to macroscopic values because of the diverging in-layer correlation length.

Many experiments have been performed on the pure compounds.[1] Of relevance here are those in the archetypal 2D Ising antiferromagnet Rb_2CoF_4, whose critical exponents were found to be in excellent agreement with those of the exact Onsager analytical solution.[2] Also for Heisenberg-like systems Ising critical behavior was observed,[3] which is ascribed to the presence of the small crystalline anisotropy stabilizing the fluctuations along the c axis. Furthermore, various randomly diluted[4] and randomly mixed[5] antiferromagnets were investigated, and their magnetic properties were found to be in conformity with Ising critical behavior.

A number of theoretical predictions were made of the effect of adding magnetic impurities on the critical phenomena. The widely used criterion by Harris[6] tells that the critical exponents of a magnetic system with a small amount of added impurities remain unchanged if the exponent α of the specific heat of the pure system is negative, but that the critical behavior is modified upon approaching the transition if α is positive. Later theoretical studies and computer simulations have supported this finding.[7] For the present system, $Rb_2Cu_{0.12}Co_{0.88}F_4$ ($S_{Cu} = \frac{1}{2}$, $S_{Co} = \frac{1}{2}$), which should conform to the $S = \frac{1}{2}$ Ising spin model, α is zero, and so the Harris criterion is not applicable. For the case of nonmagnetic impurities, i.e., magnetic dilution, careful computer simulations indicate that the critical behavior is identical to that of the pure case except for small logarithmic corrections very near to T_c.[8] No firm conclusions have, however, been reached[9,10] for the ordering in the case of mixed ferromagnetic and antiferromagnetic interactions, which result in a complex phase diagram.

Experiments on the diluted 2D Ising antiferromagnet $Rb_2Co_xMg_{1-x}F_4$ furthermore showed the remarkable feature that the development of the 3D correlations at the Néel temperature T_N strongly depends on the cooling rate through the transition.[11] It is to be noticed that this effect can only be observed in Ising systems, where below the transition the energy barrier that must be surmounted to flip a domain is high enough for the associated relaxation times to exceed the typical cooling times, which are of the order of seconds.

The present neutron-scattering study is primarily aimed at the critical behavior of $Rb_2Cu_{0.12}Co_{0.88}F_4$, which is a 2D Ising antiferromagnet that is perturbed by admixture of ferromagnetic interactions. Admixture of exchange interactions of opposite sign adds a completely new element to the study of critical behavior of 2D magnetic systems, viz., frustration of the interactions within the square magnetic lattice. For Cu concentrations x up to a few tens of percent, the system $Rb_2Cu_xCo_{1-x}F_4$ is still far away from the transition to a spin glass. This transition does not occur until $x \approx 0.60$.[12] In addition, ordering phenomena already show up at temperatures as high as ≈ 100 K, whereas 2D spin glasses have a vanishing critical temperature.[13] Around $T_N = 88.1 \pm 0.1$ K, therefore, the present system is remote from any reentrant spin-glass phase, such as has been observed in the mixed 3D ferromagnet-antiferromagnet $Eu_xSr_{1-x}S$,[14] and predicted to exist by theoretical arguments[15] and computer simulations.[16] Below, it is found that the critical behavior of $Rb_2Cu_{0.12}Co_{0.88}F_4$ is Ising for small length scales, yet that the system fails to achieve genuine long-range order below the onset of the sublattice magnetization at T_N. A rearrangement of the domains to larger ones as well as temporal effects associated with this rearrangement are observed in a relatively wide regime of temperatures below T_N.

II. EXPERIMENTAL DETAILS

The single crystal of $Rb_2Cu_{1-x}Co_xF_4$ used in the experiments, having a Co content $x = 0.88$, was grown along the c axis by the Czochralski pulling technique, as described in Ref. 12. It measures $4 \times 5 \times 1.5$ mm^3, with the larger faces parallel to the magnetic layers. The variation in x is estimated to be about 1%, corresponding to a spread in T_N of approximately ± 1 K. The exchange interaction constants J of the Co-Co and Cu-Cu bonds are known from the relevant pure compounds to amount to -90.8 K (Ref. 17) and 22.0 K (Ref. 18). The J of the Co-Cu bonds depends on the direction of the Cu d-orbital lobes relative to the bond axis, and is either ferromagnetic or antiferromagnetic. These J have been estimated to be ~ -37 K and ~ 20 K.[19]

The neutron-scattering experiments were performed on the TAS1 spectrometer at the cold-source facility of the DR3 reactor of the Risø National Laboratory, Denmark. The momentum transfer was chosen in the (a^*, c^*) plane. Incident neutron energies of 5 and 20 meV were used. At 5 meV ($k_F = 1.565$ Å^{-1}), the spectrometer was operated in the two-axis configuration with a horizontal collimation of 60′ between monochromator and sample and 120′ between sample and detector. The effective horizontal collimation before the monochromator crystal was 1°. Second-order reflections were eliminated by the use of a liquid-nitrogen-cooled Be filter. At 20 meV ($k_F = 3.129$ Å^{-1}), the second-order reflection of the pyrolytic graphite monochromator was utilized, giving adequate energy resolution while maintaining the scattering angle of the monochromator. Here, the first-order 5-meV neutrons were filtered out by use of an analyzer selecting 20-meV neutrons in first order, but made broadband by eliminating all collimation between analyzer crystal and detector. The horizontal collimation from monochromator to analyzer was 30′-30′. Additionally, a number of experiments were performed at 10 meV ($k_F = 2.197$ Å^{-1}) on the TAS7 spectrometer in the two-axis configuration. Here, higher-order energies are largely filtered out by the neutron guide tube. The low temperatures were maintained by use of a cryostat equipped with a closed-cycle helium refrigerator. From the nuclear Bragg reflections the magnetic unit cell dimensions were found to be $a = 4.16\sqrt{2}$ Å and $c = 13.72$ Å at 4.2 K. From the width of these reflections, the mosaic spread about the c axis was derived to be less than $\pm 0.1°$.

III. RESULTS

A. Critical scattering

To measure the critical scattering, we performed, at fixed temperatures, scans $\mathbf{Q} = (h, 0, 0.41)$ across one of the 2D-associated magnetic ridges at 20 meV incident neutron energy (Fig. 1), and scans $\mathbf{Q} = (h, 0, 0.60)$ at 10 meV energy. At the central $\mathbf{Q}$ of these scans, the outgoing neutron beam points along the c axis, i.e., along the diffusive rod, which ensures integration over the energy in fulfillment of the quasielastic approximation.[20]

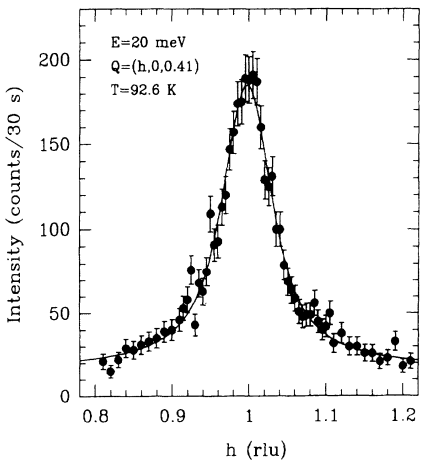

FIG. 1. Scan $\mathbf{Q} = (h, 0, 0.41)$ across the critical ridge at 92.6 K. Incident neutron energy is 20 meV. The solid line is a fit of Eq. (3) convoluted with the instrumental resolution and augmented with a background.

The spectral differential cross section for scattering of unpolarized neutrons is quite generally given by

$$\frac{d^2\sigma}{d\Omega d\omega} \propto |f(\mathbf{Q})|^2 \sum_{\alpha,\beta} (\delta_{\alpha\beta} - \hat{Q}_\alpha \hat{Q}_\beta) S^{\alpha\beta}(\mathbf{Q},\omega) \ , \quad (1)$$

where $\alpha,\beta = x,y,z$, $\mathbf{Q} = (hkl) = \mathbf{q}_f - \mathbf{q}_i$, with $\mathbf{q}_i$ and $\mathbf{q}_f$ denoting the initial and final neutron wave vectors, and $f(\mathbf{Q})$ is the form factor. The wave-vector-dependent response function $S^{\alpha\beta}(\mathbf{Q},\omega)$ is the space-time Fourier transform of the spin-pair correlation function $\langle S_0^\alpha(0) S_\mathbf{r}^\beta(t)\rangle$. Above T_N, where Bragg scattering is absent, the fluctuation-dissipation theorem relates the average spin correlation function $\langle S_0^\alpha(0) S_\mathbf{r}^\beta(t)\rangle$ to the wave-vector-dependent susceptibility $\chi^{\alpha\alpha}(\mathbf{Q})$. When integrating over ω in the limit $\hbar\omega \ll k_B T$, such as is done by the instrument at the ridge $\mathbf{Q}$ specified above, the differential cross section due to critical scattering reads

$$\left(\frac{d\sigma}{d\Omega}\right)_{\text{crit}} \propto |f(\mathbf{Q})|^2 \frac{k_B T}{g^2 \mu_B^2} \chi^{\alpha\alpha}(\mathbf{Q}) \ . \quad (2)$$

The susceptibility is usually approximated by the Fisher-Burford approximant[21]

$$\chi^{zz}(\mathbf{Q}) = \frac{A(T)}{(\kappa^2 + q^2)^{1-\eta/2}} \ , \quad (3)$$

where $\mathbf{q}$ is the wave vector with reference to the ridge $\mathbf{Q}$, κ is the inverse in-plane correlation length, $A(T)$ is dependent on the temperature only, and $\eta = 0.25$ according to theory.[21]

The measured ridge profiles were analyzed, for each temperature, by least-squares fitting Eq. (2) with Eq. (3) inserted and folded with the instrumental resolution function. The latter was identified with the profile measured at low temperatures ($\sim$ 20 K), where the ridge is resolution limited as it exclusively results from the magnetic Bragg scattering associated with imperfect stacking among the layers (cf. Figs. 2 and 3). This profile is confirmed by the profiles resulting from reworking the instrumental profiles measured at the nearby nuclear Bragg reflections (200) and (020) to the relevant $\mathbf{Q}$ and integrating them over the c^* direction. Notice that $f(\mathbf{Q})$ varies only weakly over the scans. The quantity η was set to its theoretical value because the data do not permit an accurate determination. We note, however, that the fits improved slightly upon taking somewhat higher values for η (up to 0.5). The fits yielded values for χ^2 ranging from 0.9 to 1.3. A typical fit is shown in Fig. 1. The results for the inverse correlation length κ are presented versus the temperature in Fig. 2 for 20 meV incident neutron energy.

As is observed from Fig. 2, the development of the inverse in-layer correlation length κ with the temperature shows a number of remarkable features: (i) Above $T_N = 88.1$ K, here defined by the onset of the sublattice magnetization (see below), κ varies essentially linearly with temperature, as is appropriate for a 2D Ising system. (ii) κ does not vanish at T_N, but stays finite. At T_N, it has reached a value of 0.011 reciprocal lattice units (rlu), which corresponds to ordered domains of

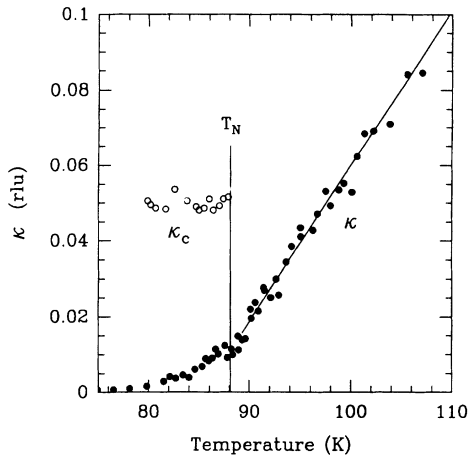

FIG. 2. Temperature dependence of the inverse in-plane correlation length κ (solid circles), extracted from scans $\mathbf{Q} = (h,0,0.41)$ across the ridge (cf. Fig. 1) by use of Eq. (3), and the inverse intralayer correlation length κ_c (open circles), derived from scans $\mathbf{Q} = (10l)$ along the ridge by use of Eq. (8). Incident neutron energy is 20 meV. The solid line is a fit of Eq. (4).

only 14 lattice spacings in linear size. (iii) Upon lowering the temperature below the transition, κ keeps decreasing and ultimately vanishes within errors around 75 K. Its slope at the same time tends to zero. We emphasize that apart from small time-dependent effects (cf. Sec. III C), the relationship of κ on the temperature in Fig. 2 is not history dependent. That is to say, on coming from low temperatures the long-range-ordered domains break up into smaller ones above about 75 K.

Because the system orders in finite domains rather than that it attains true long-range order, we analyze κ above T_N in terms of the standard power law augmented with a temperature-independent contribution κ_1 allowing for the finite domain size. That is,

$$\kappa = \kappa_0 \left(\frac{T - T_N}{T_N}\right)^\nu + \kappa_1 \ , \quad (4)$$

where κ_0 and κ_1 are constants. Equation (4) is admittedly heuristic, but finds some justification in the argument that the frustration especially affects the long-ranged excitations, which are heavily suppressed. A lower bound of κ, therefore, is imposed on the system at all temperatures above T_N. A similar partition of κ has been used in connection with percolation[22] and random fields.[23] In fitting Eq. (4) to κ, we furthermore realize that the system exhibits a finite spread in T_N, which in anticipation of the analysis of the sublattice magnetization below is represented by the Gaussian distribution $A \exp[(T_N - \langle T_N\rangle)^2/2\sigma^2]$, with $\langle T_N\rangle = 88.1$ K and $\sigma = 0.65$ K. The fits to the experimental κ above 90 K then yield $\nu = 1.00 \pm 0.04$, $\kappa_0 = 0.36 \pm 0.03$ rlu, and $\kappa_1 = 0.011 \pm 0.001$ rlu for the 20-meV data. The 10-meV data similarly yield $\nu = 1.06 \pm 0.05$, $\kappa_0 = 0.32 \pm 0.04$ rlu, and $\kappa_1 = 0.011 \pm 0.002$ rlu. The weighted averages are $\nu = 1.02 \pm 0.04$, $\kappa_0 = 0.34 \pm 0.03$ rlu, and

$\kappa_1 = 0.011 \pm 0.002$ rlu. It is noted that these results are highly insensitive to σ since ν is so close to unity. In fact, if we ignore the spread in T_N ($\sigma = 0$), we find values for ν, κ_0, and κ_1 differing by only a minor fraction of the errors quoted.

The intensity of the ridge was measured in separate runs as a function of the temperature. These data were taken at $\mathbf{Q} = (1,0,0.41)$ for 20 meV, at $\mathbf{Q} = (1,0,0.60)$ for 10 meV, and at $\mathbf{Q} = (1,0,0.70)$ for 5 meV incident neutron energy. The experimental data for 10 and 20 meV are given in Fig. 3. The ridge intensity is seen to increase upon approaching T_N from above, but remarkably does not drop after passing through the transition. Instead, the amplitude levels off for a few kelvin (see inset to Fig. 3), and subsequently rises further. As pointed out above, the ridge at the same time narrows down because of the further growth of the domains in the layers, to become essentially resolution limited below 75 K. The obvious explanation is that the critical scattering, which dies out below T_N, is gradually replaced by a magnetic Bragg ridge developing from T_N downwards. It is pointed out in connection with Fig. 2 that the critical part of the scattering does not diverge.

The quantity $\chi^{zz}(0)$ has been derived as a function of the temperature from the ridge profiles at 10 and 20 meV, which were already analyzed in connection with the determination of κ. Here, the data in Fig. 3 above T_N, which were collected in single runs, were used to check the peak intensities of the ridge profiles at the various temperatures with one another. The results are given in Fig. 4. Because of the predominantly Ising nature of the interactions, the transverse susceptibility presumably does not contribute significantly to the divergence. Its contribution will henceforth be ignored, upon noting that residual effects of the transverse susceptibility would slightly enhance the derived γ. It seems attractive, of course, to deduce the critical exponent γ pertaining to

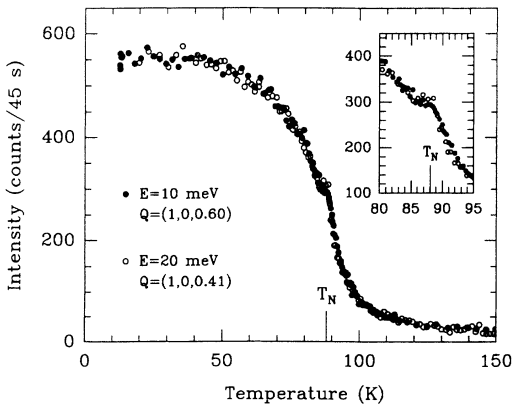

FIG. 3. Peak intensity of the ridge vs the temperature. Solid circles refer to $\mathbf{Q} = (1,0,0.60)$ at 10 meV and open circles to $\mathbf{Q} = (1,0,0.41)$ at 20 meV incident neutron energy. The inset shows the critical regime to better advantage. Below $T_N = 88.1$ K, the intensity arising from a magnetic Bragg ridge takes over from the critical scattering, indicative of the absence of long-range order along the c axis.

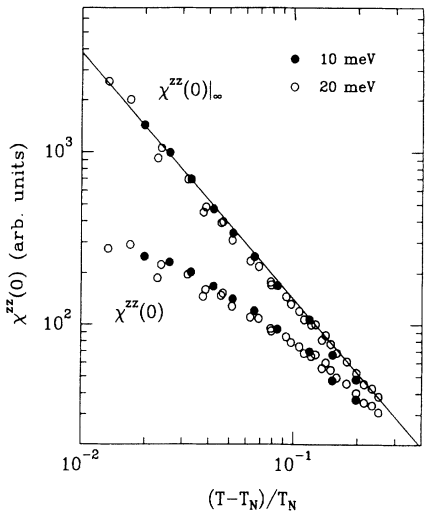

FIG. 4. Double-logarithmic plot of the susceptibility $\chi^{zz}(0)$ vs the reduced temperature. Solid circles refer to 10 meV, open circles to 20 meV incident neutron energy. The lower traces represent $\chi^{zz}(0)$, i.e., the ridge peak intensity after deconvolution for the instrumental resolution. The upper traces represent $\chi^{zz}(0)|_\infty$, Eq. (6), in which account is given of the finite correlation length at the transition.

the divergence of $\chi^{zz}(0)$, i.e., $\chi^{zz}(\mathbf{Q})$ at $q = 0$, by fitting the power law

$$\chi^{zz}(0) \propto \left(\frac{T - T_N}{T_N}\right)^{-\gamma} \tag{5}$$

to the results for $\chi^{zz}(0)$ in Fig. 4. In doing so, however, we readily discover that the fit is of poor quality and that the derived $\gamma = 0.9 \pm 0.2$ (Ref. 24) bears no resemblance to the 2D Ising value $\gamma = \frac{7}{4}$. The fits also do not markedly improve upon accounting for the spread in T_N.

It is reasonable to suppose that the slow divergence of $\chi^{zz}(0)$ is related to the paucity of small-wave-vector fluctuations in the frustrated system. To provide some confirmation for this, we have reworked at each temperature the measured $\chi^{zz}(0)$ to the value $\chi^{zz}(0)|_\infty$ which $\chi^{zz}(0)$ would have had if κ_1 were zero. According to Eq. (3) with $q = 0$ and Eq. (4), we have

$$\chi^{zz}(0)|_\infty = \chi^{zz}(0)\left(\frac{\kappa_0\epsilon^\nu + \kappa_1}{\kappa_0\epsilon^\nu}\right)^{2-\eta}, \tag{6}$$

in which $\epsilon = (T - T_N)/T_N$ is the reduced temperature. The results for $\chi^{zz}(0)|_\infty$ are displayed in Fig. 4, where in Eq. (6) use is made of $\eta = 0.25$ and the average ν, κ_0, and κ_1 deduced above. The enhancement of $\chi^{zz}(0)$ is self-evidently minimal at higher temperatures, but rises towards a factor 4.6 at 90 K. When fitting the power law to $\chi^{zz}(0)|_\infty$ rather than to $\chi^{zz}(0)$, we find $\gamma = 1.5 \pm 0.2$ for both the 10-meV and the 20-meV data. Again, account was given of the finite spread in T_N. The fits to $\chi^{zz}(0)|_\infty$ are also entered in Fig. 4 as the straight line. The result for γ compares within errors with the val-

ues found in 2D Ising systems without frustration. The agreement is perhaps to some extent fortuitous because Eq. (6) lacks a firm theoretical basis, but it definitely confirms that the tendency of the system to form domains impedes the development of long-range fluctuations.

B. Bragg scattering

We first discuss the finite correlation among the layers along the c axis. In order to measure these, we have performed scans $\mathbf{Q} = (10l)$ at various temperatures. Figure 5 shows two scans, one above T_N at 91.0 K, and one at low temperature at 13 K obtained after slow cooling through T_N. In the former, the scattering intensity is virtually constant apart from the decrease of the neutron form factor with increasing l, which confirms that the ordering processes are essentially 2D in nature. The latter scan shows magnetic Bragg peaks at $l = 0, 1, 2$, etc., which however are substantially broadened because of the very limited correlation along the c axis. Note that this is quite different from what one sees in pure square-lattice systems, which are known to acquire long-range order in 3D once order in the layers is achieved. From the width of the peaks along the rod, the inverse correlation length κ_c along the c axis has been deduced under the simplifying assumption that these correlations fall off with distance according to the single-exponential function $\exp(-\kappa_c c)$. In this case, the structure factor $\mathcal{F}(Q_z)$ with due account of the diminishing c-axis correlations may for all κ_c be derived in analytical form by performing the *discrete* Fourier transform of $\exp(-iQ_z z - \kappa_c|z|)$ summed over all layers including the ones at half-integer lattice displacements along the c axis. The result is

$$\mathcal{F}(Q_z) = \frac{\sinh(\kappa_c c)}{\cosh(\kappa_c c) - \cos(Q_z c)} \times [1 + \sigma_d \exp(-\tfrac{1}{2}\kappa_c c)\cos(\tfrac{1}{2}Q_z c)] , \quad (7)$$

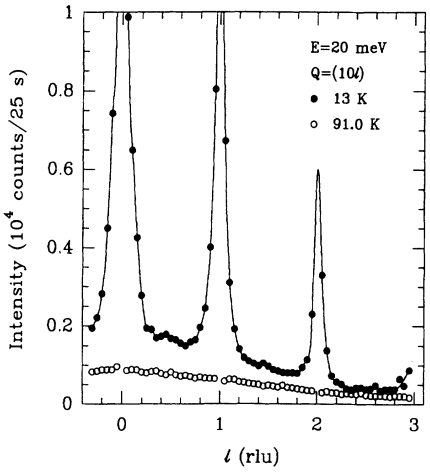

FIG. 5. Ridge intensity for scans $\mathbf{Q} = (10l)$ along the ridge at 91.0 K (open circles) and 13 K (solid circles) at 20 meV incident neutron energy. At 91.0 K the intensity of the critical scattering is constant apart from the form factor, indicative of the 2D nature of the critical scattering. Drawn line is a guide to the eye.

with $\sigma_d = \pm 1$ according to the type of domain. The latter differ only in the sign of the sublattices on the half-integer layers, and may alternatively be distinguished by whether the (a, c) planes or the (b, c) planes are ferromagnetically ordered. Note that a single domain provides Bragg scattering at either even or odd l. Averaged over the two domain types, we are left with[25]

$$\mathcal{F}(Q_z) = \frac{\sinh(\kappa_c c)}{\cosh(\kappa_c c) - \cos(Q_z c)} . \quad (8)$$

For $\kappa_c c \ll 1$, which is fulfilled in the case of the data at 13 K, Eq. (8) returns to the Lorentzian form

$$\mathcal{F}(Q_z) = \frac{2\kappa_c/c}{\kappa_c^2 + q_z^2} . \quad (9)$$

Analysis of the Bragg ridge at 13 K yields that $\kappa_c = 0.06 \times 2\pi/c$ after moderately slow cooling through T_N; i.e., the interplanar correlation amounts to about 2.6 in units of c. No appreciable change in κ_c was found from the onset of the peaks at T_N (cf. Fig. 2) all the way down to 13 K, so that the interplanar correlations remain several orders of magnitude smaller than the correlations within the planes. Also in the ordered regime, therefore, the system must be considered to be truly 2D, and even more so than nonfrustrated 2D systems.

To determine the order parameter, i.e., the sublattice magnetization, as a function of the temperature, and to derive a critical exponent β from it, we have measured the intensity of the magnetic Bragg scattering at the reciprocal lattice point $\mathbf{Q} = (101)$ at incident neutron energies of 5, 10, and 20 meV. The onset of magnetic scattering occurs at about 88 K. The antiferromagnetic axial ordering is consistent with the absence of magnetic Bragg intensity at $\mathbf{Q} = (002)$ and (004) [cf. Eq. (1)]. In the regime of temperatures just below the transition (75–88 K), where the order gradually becomes of longer range, the magnetic Bragg peak is not yet resolution limited within the planes. In fact, the in-plane width of the Bragg peak equals, within errors, the width of the ridge below T_N (cf. Fig. 2). This implies that we must correct for the folding of the Bragg peak with the instrumental resolution function in the q_x and q_y directions. No correction needs to be made for integration over q_z since κ_c is independent of the temperature (cf. Fig. 2). Integration over q_y is ensured by the minimal vertical collimation of the spectrometer (5°). To integrate over q_x we adopt a Lorentzian shape for the unfolded Bragg peak and assume that the instrumental resolution function is adequately described by a Gaussian. The quantity we are interested in, the integrated Bragg intensity I_{Bragg}, may then be recovered from the measured peak intensity I_{meas} by the use of

$$I_{\text{meas}} = \int \exp\left(-\frac{q_x^2}{2\sigma_{\text{res}}^2}\right) \frac{\kappa I_{\text{Bragg}}}{\pi(\kappa^2 + q_x^2)} dq_x , \quad (10)$$

which is defined such that $I_{\text{Bragg}} = I_{\text{meas}}$ in the limit of small κ ($\kappa \ll \sigma_{\text{res}}$). Here, the minor contribution to I_{meas} arising from the critical scattering must self-evidently be subtracted out. It may be estimated to sufficient accuracy from the measured intensity at the ridge positions of

Q (Fig. 3) by scaling to the relevant Bragg position with the aid of Fig. 5 to account for the slightly different form factor. Note that κ is temperature dependent (cf. Fig. 2) and becomes vanishingly small below 75 K, and so no correction is required below this temperature. Given $\sigma_{\rm res}$ for the relevant spectrometer setting, we have inserted the measured κ for each temperature into Eq. (10). The results for $I_{\rm Bragg}$ are displayed in Fig. 6 as a function of the temperature.

Below the transition temperature $I_{\rm Bragg}(T)$ should scale with the sublattice magnetization squared, and follow the power law

$$I_{\rm Bragg}(T) \propto \left(\frac{T_N - T}{T_N}\right)^{2\beta} , \qquad (11)$$

with β the critical exponent of the order parameter. We make the reasonable assumption that T_N is distributed according a Gaussian distribution, so that

$$I_{\rm Bragg}(T) \propto \frac{1}{(2\pi\sigma)^{1/2}} \int \left(\frac{T_N - T}{T_N}\right)^{2\beta} \times \exp\left(-\frac{(T_N - \langle T_N\rangle)^2}{2\sigma^2}\right) dT_N . \qquad (12)$$

Fits of Eq. (12) to the 5-meV data in Fig. 6 above 78 K then yield the results $\beta = 0.16 \pm 0.04$, $\sigma = 0.65 \pm 0.10$ K, and $T_N = 88.1 \pm 0.1$ K. Quite similar results are found from the 10-meV and 20-meV data. The errors mainly reside in the uncertainties of the correction by Eq. (10). The fit is also entered in Fig. 6. The noteworthy result is that the β found is in conformity with the 2D Ising value $\beta = \frac{1}{8}$ although the magnetization originates from finite domains rather than from an infinite cluster. On the other hand, it should be appreciated that upon lowering the temperature the order parameter takes longer to reach its saturation value than it does in regular 2D Ising systems.

C. Nonequilibrium behavior

The presence of frustrated sites leads to a pinning of domain walls, and as a result long-wavelength correlations can only be excited at high energy cost. One of the consequences is a substantial slowing down of the ordering kinetics. This is reminiscent of the spin-glass phase occurring in $Rb_2Cu_{1-x}Co_xF_4$ for $0.18 < x < 0.40$, where the relaxation times have been found to be distributed over more than ten decades.[13] Below T_N, therefore, time effects should occur. The spectrum of relaxation times is expected to be broad and to extend to very long time scales, even beyond those associated with the experimental time window (~ 1 s). In other terms, when cooled to a certain temperature, the system will not reach the equilibrium state associated with that temperature if the passage through the transition is fast enough for the slower processes to be ineffective.

We have investigated these effects first by observing to what extent the intralayer and in-layer correlations depend on the cooling rate. The experimental method is to measure the width of a magnetic Bragg peak along the c^* and a^* directions, respectively.[11] As concerns the correlations among the layers, in Fig. 7 two scans over the (101) Bragg peak are presented, both taken at 80 K, where the relaxation presumably is exceedingly slow. One scan was obtained after cooling through the transition at a rate of 3 K/min, and the other scan after cooling through the transition at a rate of 0.25 K/min. Slower cooling is seen to lead to a markedly better stacking of the layers, but the slower cooling rate is not yet slow enough to achieve long-range order. After deconvolution for the instrumental resolution as determined from nearby nuclear Bragg peaks, Eq. (8) was found to fit the two data sets for $\kappa_c = 0.054$ and 0.039 rlu, corresponding to correlation lengths of 3.0 and 4.1 in units of c, respectively. Note

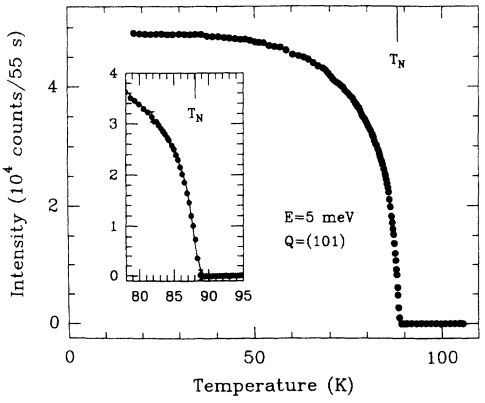

FIG. 6. Integrated intensity of the domain-broadened magnetic Bragg peak at $\mathbf{Q} = (101)$ vs the temperature for 5 meV incident neutron energy. The data points are derived from the measured peak intensities and the κ in Fig. 2 by use of Eq. (10). The minute contribution arising from critical scattering has been subtracted.

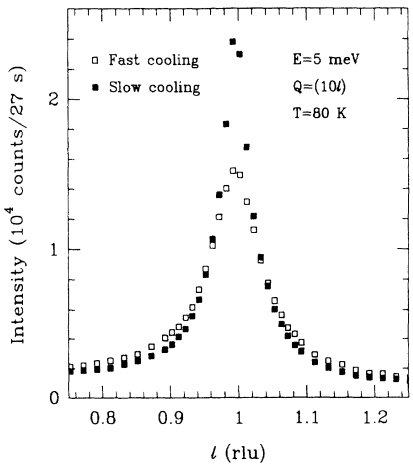

FIG. 7. Magnetic Bragg intensity for scans along the c^* axis through the Bragg point $\mathbf{Q} = (101)$ at $T = 80$ K after slow cooling and after fast cooling through T_N. After fast cooling a shorter correlation length is observed along the c axis. The drawn curves are fits to Eq. (8). The data are taken at 5 meV incident neutron energy.

that the intensity in the wings does not drop to zero, which is due to the presence of the magnetic Bragg ridge along the c^* axis at the relevant temperature.

To probe the effects of cooling on the in-layer correlations, we performed similar scans through the same Bragg peak along the a^* axis. The results are given in Fig. 8, in which the fast-cooling data have been scaled to the same peak intensity as the slow-cooling data. Although both peaks in Fig. 8 are near being resolution limited due to the large spatial extent of the in-layer correlations (cf. Fig. 2), a significant difference is found in the wings, evidence that also in the planes the correlation length has not reached its equilibrium value. This is in sharp contrast with the case of diluted antiferromagnets,[22] where a breakup of the long-range order within the planes was only observed to occur very close to the percolation threshold. The minor broadening of the Bragg peak after fast cooling as compared to the one after slow cooling allows one to extract an upper estimate of ~ 200 lattice spacings for the correlation length after fast cooling.

A second experiment concerns proving, although only qualitatively, that the spectrum of relaxation times is very broad. Here, reliance is made on the reasonable assumption that this spectrum shifts by many orders of magnitude when passing through a narrow temperature interval around T_N. The experiment is set up as follows. First the system is cooled slowly (0.2 K/min) to a certain temperature T_q around T_N, after which a fast quench (3 K/min) is applied down to 80 K. Subsequently, the (101) Bragg profile is measured along the ridge to determine the correlation length along the c^* axis as frozen in at T_q. The results deduced for the inverse correlation length κ_c measured after cooling to 80 K are collected as a function of T_q in Fig. 9. To appreciate this figure, note that the upper asymptotic level is the final κ_c after cooling from a "high" temperature to 80 K at a rate of 3 K/min; similarly, the lower asymptotic level corresponds to the κ_c reached after cooling all the way down at 0.2 K/min. Faster cooling below T_q would lower the final κ_c, but would not appreciably alter the "width" of the S-shaped curve in Fig. 9. The data can be parametrized in terms of an error function corresponding to a full width at half maximum of 2.5 K. This is significantly wider than the spread resulting from the inhomogeneity in T_N, which has a full width half maximum of $2(2\ln 2)^{1/2} \times 0.65 = 1.5$ K [cf. Fig. 10 and Eq. (12)]. It takes about 1 K, therefore, for the spectrum of relaxation times to pass through our experimental time window, which provides the argument for the broadness of the relaxation time spectrum.

It is tempting to follow the growth of the correlation length via the development with time of the profiles of magnetic Bragg peaks or the magnetic Bragg ridge, which takes over from the critical ridge scattering below 80 K. Here, we must distinguish between correlations along the c axis and those in the planes. Increase in the correlation length along the c axis will result in a decreasing intensity of the Bragg ridge and an increasing intensity of the Bragg peaks, whereas increase in the correlation length in the planes will result in an increase in the intensities of both the Bragg ridge and the Bragg peaks. It has already been pointed out that the in-plane correlations grow with decreasing temperature down to ~ 75 K (cf. Fig. 2), whereas the c-axis correlations, although markedly dependent on the cooling rate through T_N, do not appreciably grow below, say, 79 K.

We first consider the temporal development of the c-axis correlations. Following a quench in temperature from 100 K down to 87.8 K, we performed repetitive scans across the (101) point in the c^* direction. The

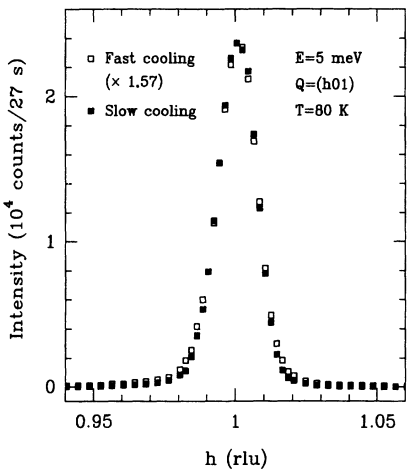

FIG. 8. Magnetic Bragg intensity for scans along the a^* axis through the Bragg point $\mathbf{Q} = (101)$ at $T = 80$ K after slow and fast cooling through T_N. The fast-cooling data have been scaled to the same peak intensity as the slow-cooling data to facilitate a comparison of the wings. In the wings, a small but significant difference is observed, indicating that the correlations within the planes extend further out upon slow cooling. The data are taken at 5 meV incident neutron energy.

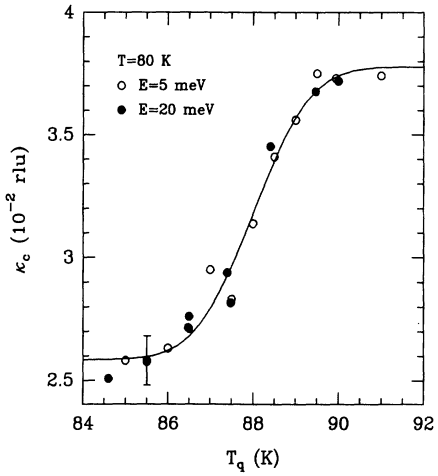

FIG. 9. Inverse correlation length κ_c along the c axis, derived from (101) Bragg profiles, after slow cooling to T_q followed by a quench to 80 K. The drawn line is a fit to an error function. Incident neutron energy is 5 meV (open circles) or 20 meV (solid circles).

recorded Bragg profiles were deconvoluted for the instrumental resolution upon adopting a scattering function of the form specified in Eq. (8). The extracted peak intensities and inverse interplanar correlation lengths κ_c are plotted in Fig. 10 vs the time elapsed since the quench. A distinct increase is observed in the peak intensity and a corresponding decrease of κ_c, the integrated intensity remaining constant within errors. The effect amounts to about 40% in a time span of three hours. Both the peak intensity and κ_c, therefore, signify that the interlayer correlations have lengthened by that amount, which constitutes very direct evidence for domain growth along the c axis in the present frustrated system. It is noted that the smallest κ_c entered in Fig. 10, measured at 400 s, is larger than the κ_c measured at lower temperatures after fast cooling (cf. Fig. 9). This is presumably caused by the appreciable growth of the correlations in the time needed to complete the first scan.

We now turn to the in-plane correlations, the growth of which is much more difficult to probe because of the smallness of the effect (cf. Fig. 8). The effects of lengthening of interlayer and intralayer correlations on the intensity of the Bragg ridge are opposite, and so one may hope to see an increment of the intralayer correlations via a change with time of the appropriate sign. In the experiment, the sample was quenched down to 81.3 K, where the ridge is still not resolution limited, signifying that the in-plane correlations still depend on the temperature and eventually also on the time. The peak intensity was monitored at $\mathbf{q} = (1, 0, 1.4)$ up to 2×10^4 s after the quench. The result is given in Fig. 11. A small but significant *increase* is observed in the peak intensity of the Bragg ridge. This is indeed consistent with an increasing in-plane correlation length. Figure 11, therefore, confirms the effect of domain growth within the planes. The errors do not permit one to say anything definitive about the functional dependence of the lengthening. It is noted, however, that the data in Fig. 11 are consistent with a slow logarithmic growth of the correlation length, such as has been derived in Ref. 26 and recently observed observed in the ferromagnetic counterpart $Rb_2Cu_{0.89}Co_{0.11}F_4$ via the susceptibility.[27]

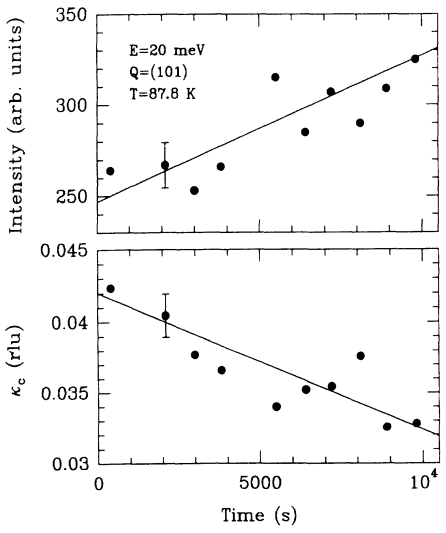

FIG. 10. Peak intensity of the (101) Bragg peak and the inverse correlation length κ_c derived from its width vs the time elapsed since a temperature quench to 87.8 K. The results indicate an improvement of the layer stacking with time. Incident neutron energy is 20 meV.

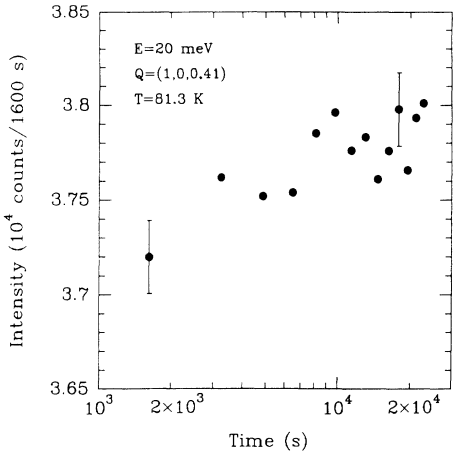

FIG. 11. Peak intensity of the ridge at $\mathbf{Q} = (1,0,0.41)$ vs the time elapsed since a quench to 81.3 K. At this temperature the intensity originates almost exclusively from magnetic Bragg scattering. The growth of the ridge intensity reflects the growth of the domains within the planes. Incident neutron energy is 20 meV.

IV. CONCLUSIONS

Critical scattering has been performed in the frustrated 2D Ising antiferromagnet $Rb_2Cu_{0.12}Co_{0.88}F_4$. The frustration arises from the admixture of ferromagnetic bonds in the percolating antiferromagnetic backbone. The reciprocal in-plane correlation length κ was found to decrease linearly with the temperature, with an exponent $\nu = 1.02 \pm 0.04$ in accordance with the exact 2D Ising value ($\nu = 1$). As opposed to nonfrustrated systems, however, κ does not vanish at $T_N = 88.1 \pm 0.1$ K, the temperature of the onset of the sublattice magnetization, reflecting the fact that the system orders into domains instead of achieving long-range order. Correcting for finite correlation remaining at T_N, we find $\gamma = 1.5 \pm 0.2$ for the critical exponent of the susceptibility. Upon further cooling below T_N, the domains continue to grow in a temperature regime extending over at least 10 K to length scales beyond the instrumental resolution. Upon subsequent heating the domains break up again. This domain growth and breakup is not entirely in equilibrium, apparently because of the presence of long time scales in the system. The sublattice magnetization within the domains follows a power law below T_N, with an exponent $\beta = 0.16 \pm 0.04$ in conformity with the 2D Ising value of $\frac{1}{8}$. The presence of nonequilibrium processes and the wide distribution of relaxation times associated with them have been established more directly from the observation that the in-plane and intraplanar correlation lengths depend on the history of cooling through T_N,

and further increase weakly with the time over periods of several hours.

ACKNOWLEDGMENTS

The authors thank Dr. K. N. Clausen at Risø for his interest and his unremitting care for the spectrometer operation. The work at Risø was financially supported by the Commission of the European Community through the Large Installation Plan. The work was furthermore supported by the Netherlands Foundation "Fundamenteel Onderzoek der Materie (FOM)" and the "Nederlandse Organisatie voor Wetenschappelijk Onderzoek (NWO)."

[1] See, e.g., the review by L. J. de Jongh and A. R. Miedema, Adv. Phys. **23**, 1 (1974).
[2] L. Onsager, Phys. Rev. **65**, 117 (1944).
[3] R. J. Birgeneau, H. J. Guggenheim, and G. Shirane, Phys. Rev. B **1**, 2211 (1970).
[4] H. Ikeda, J. Phys. Soc. Jpn. **50**, 3215 (1981), and references therein.
[5] R. J. Birgeneau, J. Als-Nielsen, and G. Shirane, Phys. Rev. B **16**, 280 (1977); H. Ikeda, T. Abe, and I. Hatta, J. Phys. Soc. Jpn. **50**, 1488 (1981).
[6] A. Brooks Harris, J. Phys. C **7**, 1671 (1974).
[7] For a review, see R. B. Stinchcombe, in *Phase Transitions and Critical Phenomena*, edited by C. Domb and J. L. Lebowitz (Academic Press, New York, 1983), Vol. 7.
[8] J.-S. Wang, W. Selke, Vl. Dotsenko, and V. B. Andreichenko, Physica A **164**, 221 (1990), and references therein.
[9] Y. Ozeki and H. Nishimori, J. Phys. Soc. Jpn. **56**, 1568 (1987), and references therein.
[10] H. Kitatani and T. Oguchi, J. Phys. Soc. Jpn. **59**, 3823 (1990).
[11] H. Ikeda, M. Hutchings, and M. Suzuki, J. Phys. C **11**, L359 (1978); H. Ikeda, *ibid.* **16**, 3563 (1983).
[12] C. Dekker, A. F. M. Arts, and H. W. de Wijn, Phys. Rev. B **38**, 11512 (1988).
[13] C. Dekker, A. F. M. Arts, H. W. de Wijn, A. J. van Duyneveldt, and J. A. Mydosh, Phys. Rev. Lett. **61**, 1780 (1988); Phys. Rev. B **40**, 11243 (1989).
[14] H. Maletta, G. Aeppli, and S. M. Shapiro, Phys. Rev. Lett. **48**, 1490 (1982); G. Aeppli, S. M. Shapiro, H. Maletta, R. J. Birgeneau, and H. S. Chen, J. Appl. Phys. **55**, 1628 (1984).
[15] D. Sherrington and S. Kirkpatrick, Phys. Rev. Lett. **35**, 1792 (1975).
[16] K. Binder, W. Kinzel, and D. Stauffer, Z. Phys. B **36**, 161 (1979).
[17] $J_{\text{Co-Co}}$ is determined from T_N [E. J. Samuelsen, Phys. Rev. Lett. **31**, 936 (1973); J. Phys. Chem. Solids **35**, 785 (1974); M. T. Hutchings, H. Ikeda, and E. Janke, Phys. Rev. Lett. **49**, 386 (1982)] with the aid of Onsager's exact result for the $d = 2$ Ising system (Ref. 2).
[18] $J_{\text{Cu-Cu}}$ is taken from $J_{\text{Cu-Cu}}$ in the isomorphic compound K_2CuF_4 [I. Yamada, J. Phys. Soc. Jpn. **33**, 979 (1972)] scaled with T_c.
[19] C. Dekker, A. F. M. Arts, and H. W. de Wijn, Phys. Rev. B **38**, 8985 (1988).
[20] J. Als-Nielsen, R. J. Birgeneau, H. J. Guggenheim, and G. Shirane, Phys. Rev. B **12**, 4963 (1975).
[21] M. E. Fisher and R. J. Burford, Phys. Rev. **156**, 583 (1967).
[22] R. A. Cowley, R. J. Birgeneau, G. Shirane, H. J. Guggenheim, and H. Ikeda, Phys. Rev. B **21**, 4038 (1980).
[23] R. J. Birgeneau, H. Yoshizawa, R. A. Cowley, G. Shirane, and H. Ikeda, Phys. Rev. B **28**, 1438 (1983).
[24] A preliminary analysis of the 10-meV data has been given in A. G. Schins, M. Nielsen, A. F. M. Arts, and H. W. de Wijn, Physica B **180 & 181**, 161 (1992). In this paper, the critical scattering was analyzed in the standard way on the basis of Eq. (4) with $\kappa_1 = 0$.
[25] B. Dikken, A. F. M. Arts, H. W. de Wijn, and J. K. Kjems, Phys. Rev. B **30**, 2970 (1984).
[26] D. A. Huse and C. L. Henley, Phys. Rev. Lett. **54**, 2708 (1985).
[27] A. G. Schins, A. F. M. Arts, and H. W. de Wijn, Phys. Rev. Lett. **70**, 2340 (1993).